Macroscopic acoustoelectric charge transport in graphene

L. Bandhu, L. M. Lawton, and G. R. Nash[a)]
College of Engineering, Mathematics and Physical Sciences, University of Exeter, Exeter EX4 4QF, United Kingdom

We demonstrate macroscopic acoustoelectric transport in graphene, transferred onto piezoelectric lithium niobate substrates, between electrodes up to $500\,\mu m$ apart. Using double finger interdigital transducers we have characterised the acoustoelectric current as a function of both surface acoustic wave intensity and frequency. The results are consistent with a relatively simple classical relaxation model, in which the acoustoelectric current is proportional to both the surface acoustic wave intensity and the attenuation of the wave caused by the charge transport. © 2013 AIP Publishing LLC.
[http://dx.doi.org/10.1063/1.4822121]

The electric fields associated with a surface acoustic wave (SAW) propagating on a piezoelectric material have been extensively used over the last few decades as a contactless probe of the electronic properties of a range of nanostructures including two-dimensional electron and hole systems in both the integer[1,2] and fractional quantum Hall regimes,[3] quantum wires,[4] and quantum dots.[5] SAWs can also be used to trap and transport charge, giving rise to a direct current along the direction of the wave propagation vector. This phenomenon, called the acoustoelectric effect, has been intensively studied to produce quantized current in 1-D channels,[6] for light storage in quantum wells,[7] and to induce charge pumping in nanotube quantum dots.[8] Over the last couple of years acoustically driven current flow in semiconductor nanostructures as a means of generating or controlling single electrons and photons,[9–11] for metrology and quantum information processing, has attracted received particular attention.

Although graphene's large surface area and unique properties, including its sensitivity to single absorbed molecules,[12] means that it naturally lends itself to potential integration with SAW devices, relatively little work has so far been reported. Arsat *et al.*[13] deposited graphene like nano-sheets, prepared by the reduction of graphene oxide, onto $LiTaO_3$ SAW devices and used these to sense hydrogen and carbon monoxide. The effects of moisture adsorbed on 200 nm multilayer graphene sheets and the resulting SAW attenuation was investigated experimentally by Ciplys *et al.*,[14] and we have previously investigated gas loading of graphene-quartz SAW devices.[15] Thalmeier *et al.*[16] and Zhang *et al.*[17] have both made theoretical studies of the change in SAW propagation, on a piezoelectric substrate, due to the interaction with charge carriers in graphene. Acoustoelectric charge transport has been reported from graphene sheets transferred onto lithium niobate substrates,[18] where the current electrodes used to measure the acoustoelectric current were relatively together ($20\,\mu m$). Santos *et al.*[19] have also very recently reported charge transport in epitaxial graphene on SiC, where the interaction between the SAWs and the charge carriers was relatively weak due to the relatively small piezoelectricity of

SiC. In this manuscript, we describe acoustoelectric charge transport in graphene, as a function of both SAW frequency and intensity, in devices in which the separation of the current electrodes is more than an order of magnitude larger than in the previous work. The ability to observe acoustoelectric transport over such large areas demonstrates the feasibility of creating graphene based SAW devices for a wide range of applications.

The piezoelectric interaction between SAWs and carriers in 2D systems is usually described using a simple classical relaxation model,[2] where the attenuation per unit length, Γ, and SAW velocity shift are non-monotonic functions of the diagonal component of the conductivity tensor σ^{2D}

$$\Gamma = K^2 \frac{\pi}{\lambda}\left[\frac{(\sigma^{2D}/\sigma_M)}{1 + (\sigma^{2D}/\sigma_M)^2}\right], \qquad (1)$$

$$\frac{\upsilon - \upsilon_0}{\upsilon_0} = \frac{\Delta\upsilon}{\upsilon_0} = \frac{K^2}{2}\left[\frac{1}{1 + (\sigma^{2D}/\sigma_M)^2}\right], \qquad (2)$$

where λ is the SAW wavelength, K^2 is the piezoelectric coupling coefficient (0.056 for lithium niobate), υ_0 is the SAW velocity when the surface is shorted (approximately 4000 m/s in lithium niobate), and the attenuation coefficient has a maximum at a characteristic conductivity σ_M. For a hybrid system based on lithium niobate ($LiNbO_3$) the characteristic conductivity σ_M is approximately given by $\sigma_M = \upsilon\varepsilon_0(\sqrt{\varepsilon_{xx}^S \varepsilon_{zz}^S} + 1) = 1.25 \times 10^{-6}\,\Omega^{-1}$,[20] where ε_0 is the permittivity of free space and ε_{xx}^S and ε_{zz}^S are the dielectric constants of $LiNbO_3$ at constant stress. The loss of energy from the SAW caused by this attenuation leads to a proportional loss of momentum,[20] which appears as a force on the carrier system and is the mechanism behind the acoustoelectric effect. In a closed circuit and in the absence of a magnetic field the current density j as described by Rotter *et al.*[20] and Fal'ko *et al.*[21] reduces to

$$j = -\mu Q = -\mu \frac{I\Gamma}{\nu}, \qquad (3)$$

where μ is the carrier mobility, Q is the phonon pressure given by $Q = \frac{I\Gamma}{\nu}$, I is the SAW intensity, Γ is the attenuation

[a)]Author to whom correspondence should be addressed. Electronic mail: g.r.nash@exeter.ac.uk

coefficient, and v is the velocity of the wave. From Eq. (3) it can be seen that the acoustoelectric current will also therefore reach a maximum value when the conductivity is equal to the characteristic conductivity σ_M and will vary linearly with both the SAW intensity and SAW frequency (via the attenuation).

Commercially available CVD graphene grown on copper was transferred onto three 128° YX lithium niobate SAW delay line devices. These had an acoustic path length of 5.4 mm and two identical, uniform double-electrode input/output transducers, designed to give resonances at a number of frequencies, and with a transducer aperture of 3.25 mm. The graphene was transferred using the PMMA transfer technique,[22] where a 100 nm thick layer of PMMA was first spin coated on the Cu foil, and baked at 180 °C for 10 min. The Cu was then etched away using 0.2 M ammonium persulfate solution, leaving a thin film of PMMA on graphene floating over the surface. This film was rinsed in deionized water 8–10 times to remove any residual etchant and transferred to the lithium niobate substrate. The sample was allowed to dry at room temperature to allow proper adherence of graphene to the substrate. Finally the PMMA was washed in boiling acetone (80 °C for 30 min) leaving a graphene sheet of approximately 5 mm × 5 mm on the substrate surface between the interdigital transducers.

Characterization of graphene was undertaken using Raman spectroscopy, with a Renishaw 100mW CW 532 nm laser. Raman spectra were measured at twenty five points randomly distributed across the graphene sheet, and the average of these spectra, together with that obtained from three points measured on the bare 128° YX lithium niobate, is plotted in Figure 1(a) for the best of the devices obtained (Device 1). The 2D and G peak are at 2680 cm^{-1} and 1585 cm^{-1}, respectively, and the 2D/G peak ratio was measured to be 3.5, which is characteristic of graphene.[23] A relatively small D peak at 1337 cm^{-1}, which could be attributed to the defects caused by the unintentional doping and wrinkles formed
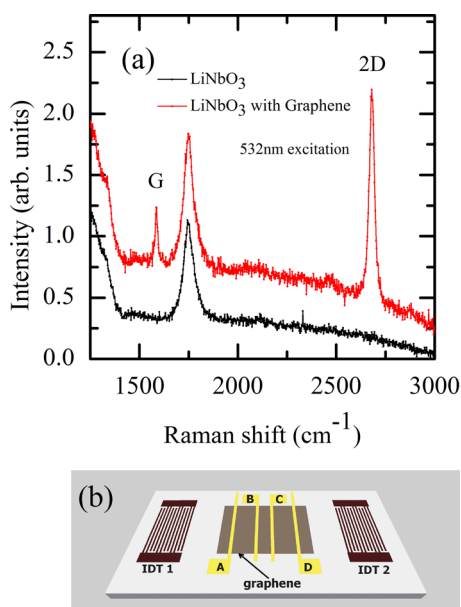

FIG. 1. (a) Raman spectrum of lithium niobate device with and without CVD graphene transferred onto the surface. (b) Schematic diagram of the device layout.

during the transfer process, suggests that the overall quality of the transferred graphene is high. 2D/G peak ratios of 3.6 and 2.2 were obtained for the second and third devices, respectively. Four metal contacts 3 mm × 20 μm were then defined (using e-beam lithography) on top of the graphene in the acoustic path as shown schematically in Figure 1(b). The separation of the outer two contacts (A and D) was 800 μm, that of the two inner contacts (B and C) was 200 μm, and the separation of the inner contacts to the outer contacts (A and B, C and D) was 300 μm. Metallization was carried out by thermal evaporation of 7 nm Cr and 70 nm Au.

The devices were mounted on a printed circuit board (PCB) using a conductive silver epoxy, and measurements were undertaken at room temperature, with the device mounted in a vacuum chamber (at a pressure of approximately 2.6×10^{-6} mbar). Measurements were made by exciting a continuous wave SAW at one transducer using an Agilent 8648C RF signal generator. The SAW amplitude at the opposing transducer was measured using a LeCroyWaveRunner 204Xi-A digital oscilloscope. The acoustoelectric current was measured using a Keithley 2400 source-measurement unit (SMU). No bias was applied between the contacts during measurement of the acoustoelectric current.

Two terminal current-voltage measurements were made at room temperature between different pairs of contacts on the three devices. For Device 1 the current was found to vary linearly with the applied bias up to voltages of 50 mV for measurements between all contacts, with measured room temperature resistance values between contacts B and D of 84 kΩ/□ and 154 kΩ/□ in air and vacuum, respectively, where the increase in resistance on evacuation of the chamber is likely to be due to the removal of adsorbed water molecules, as water is known to act as a dopant.[24] Although these values of resistance are higher of typical CVD graphene values,[25] our devices are relatively large, and it is possible that graphene is not uniform between the contacts; wrinkles, puddles, and residues arising from the transfer process could be a reason for such a large resistance. The measured resistances in Device 2 were much higher; 1.8 MΩ between contacts A and D in air, indicating that the graphene may not be continuous across the whole area. All the contacts in Device 3 were open circuit, and this device was not tested any further (contact A on Device 1 also failed in subsequent measurements).

In Figure 2(a), the measured relative SAW amplitude is plotted as a function of input frequency for Device 1, illustrating the large number of transducer harmonics, covering the range of 12 MHz up to 480 MHz that can be excited in these devices. The acoustoelectric current measured between contacts C and D for Device 1 is plotted as a function of input frequency in Figure 2(b), with an acoustoelectric current being observed at each resonance of the transducer, confirming the acoustic nature of this current. In each case a positive acoustoelectric current in the direction of SAW indicated the transport of holes, consistent with both what has been observed previously on much smaller devices[18] and the fact that CVD graphene is thought to be p-doped[26] by PMMA residues and etchant salts left behind during the transfer process. Reversing the SAW direction, by applying the RF to the opposite transducer, reversed the sign of the
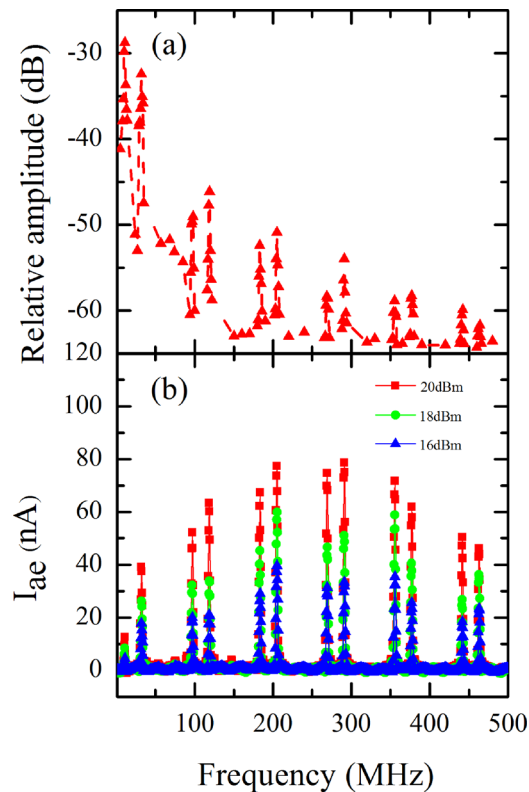
FIG. 2. (a) Measured relative SAW amplitude at different input frequencies. (b) Acoustoelectric current measured between contacts C and D on Device 1, as a function of SAW frequency and RF power.
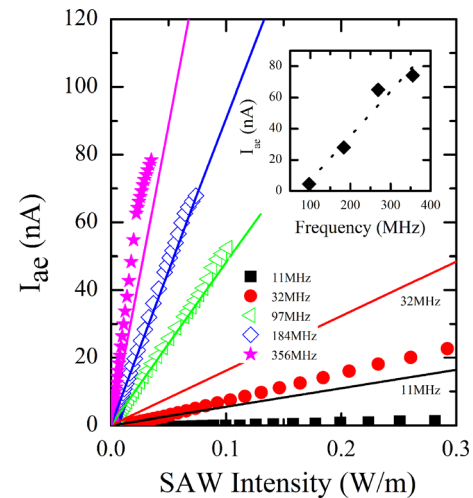

FIG. 3. Measured (symbols) and calculated (lines) acoustoelectric current as a function of SAW intensity and frequency between contacts B and C on Device 1. The inset shows the measured acoustoelectric current (symbols) as a function of SAW frequency, at a SAW intensity of 0.03 W/m, together with a linear fit to the data (dotted line).

measured current as expected. Qualitatively similar results were obtained from Device 2, which exhibited a much higher resistance, but the acoustoelectric current in this device was approximately an order of magnitude smaller under all measurement conditions. However, the behavior of the two different devices on evacuation of the chamber is consistent with the model of acoustoelectric transport based on the simple classical relaxation approach. On evacuation of the vacuum chamber, the conductivity of Device 1 decreased from $1.19 \times 10^{-5} \, \Omega^{-1}$ to $6.49 \times 10^{-6} \, \Omega^{-1}$, whereas the magnitude of the acoustoelectric current on average approximately doubled (for the same SAW frequency and intensity). As the conductivity of this device is higher than the characteristic conductivity σ_M, $1.25 \times 10^{-6} \, \Omega^{-1}$, the increase in the current is due to an increase in the attenuation (Eq. (1)) as σ_{2D} approaches σ_M (attenuation is maximum at $\sigma_{2D} = \sigma_M$). The conductivity of Device 2 decreased from $1.06 \times 10^{-6} \, \Omega^{-1}$ in air to $8.66 \times 10^{-7} \, \Omega^{-1}$ in vacuum, but in contrast to Device 1 the acoustoelectric current fell slightly (by approximately 15% on average) on evacuation of the sample chamber. As the conductivity of Device 2 is smaller than σ_M, a decrease in the conductivity also leads to a decrease in the attenuation and hence the acoustoelectric current.

In Figure 3 the acoustoelectric current measured between contacts B and D (separation 500 μm) on Device 1 is plotted as a function of SAW intensity for different SAW frequencies. At each frequency, the SAW intensity was estimated by subtracting half of the total measured insertion loss (Figure 2) from the applied RF power to the transducer. Over most of the measured range the acoustoelectric current is proportional to the SAW intensity, as predicted from the

relaxation model. In addition, the measured current is also proportional to the SAW frequency, as shown in the inset of Figure 3, where the acoustoelectric current is plotted as a function of frequency at a SAW intensity of 0.03 W/m, which is again consistent with the model. The lines in Figure 3 correspond to values of the acoustoelectric current calculated using Eq. (3) (note that the intention is not to fit to the experimental data, but rather to use the simulation to aid in the interpretation of the results). To obtain the best qualitative agreement with the measurement data, we assumed a value of the mobility of $\mu = 8 \, \text{cm}^2/\text{Vs}$ (note that the mobility could not be directly measured in our samples). As can be seen from in Figure 3, there is much better agreement between the calculated and measured values of the current at high frequencies compared to that at low frequencies. However, the non-monotonic behavior observed in both devices, as the conductivity is changed by evacuating the samples, is strong evidence that the relaxation model does describe the experimental system and was observed at all frequencies, suggesting that the model is at least partially applicable at low frequencies. One way in which better agreement between the predicted and measured values of the acoustoelectric current can be achieved is by using a smaller value of mobility for the simulations at low SAW frequencies, but it is not clear at this stage whether this is a valid approach.

The value of the mobility we have assumed is also much smaller than typical room temperature values of mobility we have obtained from 3 mm × 3 mm devices fabricated from CVD graphene transferred onto Si/SiO$_2$ substrates[27] (the corresponding hole density, approximately $5 \times 10^{12} \, \text{cm}^{-2}$ is consistent with values typically obtained from graphene on silicon). Although a different value of mobility might be expected due to the different substrate, perhaps more importantly the simple model of acoustoelectric transport described earlier does not take into account any non-uniformity of the electrical properties of the graphene (which for the very small samples studied previously would have been less important). The acoustoelectric current is dependent on the average

mobility across the device (across the transducer aperture) but is also likely to be limited by the lowest mobility the SAW encounters along its propagation path. For example, the large number of grain boundaries in the polycrystalline CVD graphene (due to the small size of the single crystal grains, which are typically a few hundred nanometers across[28]) could dramatically affect the average mobility. The measured acoustoelectric current might therefore be a useful probe of the uniformity of large graphene devices. It is also possible that the difference between the simulated and measured values of the current at long SAW wavelengths is also somehow linked to the non-uniformity of the graphene. However, much more research is required to investigate this, and work is underway to extend the classical model of charge transport to take into account of inhomogeneity in the current carrying medium. Finally, a broadly similar dependence on SAW intensity and frequency was obtained when the acoustoelectric current was measured between different contacts on the same devices. In Device 1, there was no significant difference in the size of the current measured between contacts $300\,\mu m$ and $500\,\mu m$ apart, but on average the current was approximately 30% larger when measured between the contacts closest together ($200\,\mu m$ apart). It is unclear whether this difference is also related to any potential non-uniformity in the graphene, and further work is underway to investigate the effect of varying contact separation.

In summary, we have shown that in a hybrid system of CVD graphene/LiNbO$_3$ acoustoelectric charge transport is possible over macroscopic distances, demonstrating the feasibility of graphene based SAW devices for a wide range of applications. Furthermore, by using carefully chosen SAW transducers, we show experimentally that the measured acoustoelectric current is proportional to both the SAW frequency and SAW intensity, as predicted by a relatively simple classical relaxation model. Work is underway to extend the model to take into account of the large size of these devices and any non-uniformity of the graphene.

[1]A. Wixforth, J. P. Kotthaus, and G. Weimann, Phys. Rev. Lett. **56**, 2104 (1986).

[2]A. Wixforth, J. Scriba, M. Wassermeier, J. P. Kotthaus, G. Weimann, and W. Schlapp, Phys. Rev. B **40**, 7874 (1989).

[3]See, for example, R. L. Willett, K. W. West, and L. N. Pfeiffer, Phys. Rev. Lett. **78**, 4478 (1997).

[4]G. R. Nash, S. J. Bending, M. Boero, P. Grambow, K. Eberl, and Y. Kershaw, Phys. Rev. B **54**, R8337 (1996).

[5]G. R. Nash, S. J. Bending, M. Boero, M. Riek, and K. Eberl, Phys. Rev. B **59**, 7649 (1999).

[6]J. M. Shilton, V. I. Talyanskii, M. Pepper, D. A. Ritchie, J. E. F. Frost, C. J. B. Ford, C. G. Smith, and G. A. C. Jones, J. Phys. Condens. Matter **8**, L531 (1996).

[7]C. Rocke, S. Zimmermann, A. Wixforth, J. P. Kotthaus, G. Böhm, and G. Weimann, Phys. Rev. Lett. **78**, 4099 (1997).

[8]M. R. Buitelaar, V. Kashcheyevs, P. J. Leek, V. I. Talyanskii, C. G. Smith, D. Anderson, G. A. C. Jones, J. Wei, and D. H. Cobden, Phys. Rev. Lett. **101**, 126803 (2008).

[9]O. D. D. Couto, Jr., S. Lazić, F. Iikawa, J. A. H. Stotz, U. Jahn, R. Hey, and P. V. Santos, Nat. Photonics **3**, 645 (2009).

[10]S. Hermelin, S. Takada, M. Yamamoto, S. Tarucha, A. D. Wieck, L. Saminadayar, C. Bauerle, and T. Meunier, Nature **477**, 435 (2011).

[11]A. Hernández-Mínguez, M. Moüller, S. Breuer, C. Pfuüller, C. Somaschini, S. Lazić, O. Brandt, A. García-Cristóbal, M. M. de Lima, Jr., A. Cantarero, L. Geelhaar, H. Riechert, and P. V. Santos, Nano Lett. **12**, 252 (2012).

[12]Y. Dan, Y. Lu, N. J. Kybert, Z. Luo, and A. T. C. Johnson, Nano Lett. **9**, 1472 (2009).

[13]R. Arsat, M. Breedon, M. Shafiei, P. G. Spizziri, S. Gilje, R. B. Kaner, K. Kalantar-Zadeh, and W. Wlodarski, Chem. Phys. Lett. **467**, 344 (2009).

[14]D. Ciplys, R. Rimeika, J. H. Kim, J. M. Xu, V. Chilvukula, and M. S. Shur, in IEEE Sensors Conference (2010), p. 785.

[15]E. F. Whitehead, E. M. Chick, L. Bandhu, L. M. Lawton, and G. R. Nash, Appl. Phys. Lett. **103**, 063110 (2013).

[16]P. Thalmeier, B. Dora, and K. Ziegler, Phys. Rev. B **81**, 041409(R) (2010).

[17]S. H. Zhang and W. Xu, AIP Adv. **1**, 022146 (2011).

[18]V. Miseikis, J. E. Cunningham, K. Saeed, R. O'Rorke, and A. G. Davies, Appl. Phys. Lett. **100**, 133105 (2012).

[19]P. V. Santos, T. Schumann, M. H. Oliveira, J. M. J. Lopes, and H. Riechert, Appl. Phys. Lett. **102**, 221907 (2013).

[20]M. Rotter, A. Wixforth, W. Ruile, D. Bernklau, and H. Riechert, Appl. Phys. Lett. **73**, 2128 (1998).

[21]V. I. Fal'ko, S. V. Meshkov, and S. V. Iordanskii, Phys. Rev. B **47**, 9910 (1993).

[22]X. Li, W. Cai, J. An, S. Kim, J. Nah, D. Yang, R. Piner, A. Velamakanni, I. Jung, E. Tutuc, S. K. Banerjee, L. Colombo, and R. S. Ruoff, Science **324**, 1312 (2009).

[23]A. C. Ferrari, J. C. Meyer, V. Scardaci, C. Casiraghi, M. Lazzeri, F. Mauri, S. Piscanec, D. Jiang, K. S. Novoselov, S. Roth, and A. K. Geim, Phys. Rev. Lett. **97**, 187401 (2006).

[24]T. O. Wehling, A. I. Lichtenstein, and M. I. Katsnelson, Appl. Phys. Lett. **93**, 202110 (2008).

[25]X. Li, Y. Zhu, W. Cai, M. Borysiak, B. Han, D. Chen, R. D. Piner, L. Colombo, and R. S. Ruoff, Nano Lett. **9**, 4359 (2009).

[26]A. Pirkle, J. Chan, A. Venugopal, D. Hinojos, C. W. Magnuson, S. McDonnell, L. Colombo, E. M. Vogel, R. S. Ruoff, and R. M. Wallace, Appl. Phys. Lett. **99**, 122108 (2011).

[27]C. Adlem, T. Poole, N. Mahlmeister, L. M. Lawton, and G. R. Nash, "Thermal Emission from Large Area Chemical Vapor Deposited Graphene Devices," Appl. Phys. Lett. (to be published).

[28]P. Nemes-Incze, K. J. Yoo, L. Tapasztó, G. Dobrik, J. Lábár, Z. E. Horváth, C. Hwang, and L. P. Biró, Appl. Phys. Lett. **99**, 023104 (2011).